NASA/TM–20250008723

Bondline thickness measurement from optical microscopy using image segmentation

Rodolfo Ledesma
Analytical Mechanics Associates, Hampton, Virginia

Peter Spaeth, Matthew Webster, Andrew Bergan, and Tyler Hudson
Langley Research Center, Hampton, Virginia

August 2025

NASA STI Program Report Series

Since its founding, NASA has been dedicated to the advancement of aeronautics and space science. The NASA scientific and technical information (STI) program plays a key part in helping NASA maintain this important role.

The NASA STI Program operates under the auspices of the Agency Chief Information Officer. It collects, organizes, provides for archiving, and disseminates NASA's STI. The NASA STI Program provides access to the NTRS Registered and its public interface, the NASA Technical Report Server, thus providing one of the largest collections of aeronautical and space science STI in the world. Results are published in both non-NASA channels and by NASA in the NASA STI Report Series, which includes the following report types:

- TECHNICAL PUBLICATION. Reports of completed research or a major significant phase of research that present the results of NASA programs and include extensive data or theoretical analysis. Includes compilations of significant scientific and technical data and information deemed to be of continuing reference value. NASA counterpart of peer-reviewed formal professional papers, but having less stringent limitations on manuscript length and extent of graphic presentations.

- TECHNICAL MEMORANDUM. Scientific and technical findings that are preliminary or of specialized interest, e.g., quick release reports, working papers, and bibliographies that contain minimal annotation. Does not contain extensive analysis.

- CONTRACTOR REPORT. Scientific and technical findings by NASA-sponsored contractors and grantees.

- CONFERENCE PUBLICATION. Collected papers from scientific and technical conferences, symposia, seminars, or other meetings sponsored or co-sponsored by NASA.

- SPECIAL PUBLICATION. Scientific, technical, or historical information from NASA programs, projects, and missions, often concerned with subjects having substantial public interest.

- TECHNICAL TRANSLATION. English-language translations of foreign scientific and technical material pertinent to NASA's mission.

Specialized services also include organizing and publishing research results, distributing specialized research announcements and feeds, providing information desk and personal search support, and enabling data exchange services.

For more information about the NASA STI Program, see the following:

- Access the NASA STI program home page at `http://www.sti.nasa.gov`

- Help desk contact information: `https://www.sti.nasa.gov/sti-contact-form/` and select the "General" help request type.

NASA/TM–20250008723

Bondline thickness measurement from optical microscopy using image segmentation

Rodolfo Ledesma
Analytical Mechanics Associates, Hampton, Virginia

Peter Spaeth, Matthew Webster, Andrew Bergan, and Tyler Hudson
Langley Research Center, Hampton, Virginia

National Aeronautics and
Space Administration

Langley Research Center
Hampton, Virginia 23681-2199

August 2025

Acknowledgments

We would like to thank Brandon Widener for collecting the microscopy images and the Transformational Tools and Technologies (TTT) project of the NASA Transformative Aeronautics Concepts Program (TACP) for supporting this work.

Available from:

NASA STI Program / Mail Stop 150
NASA Langley Research Center
Hampton, VA 23681-2199

Abstract

Imaging methods are attractive for bondline thickness estimation because they are fast, nondestructive, and can provide wide area coverage of a material system. However, automating the post analysis of the resulting imagery remains a challenging problem because of the need for highly accurate image segmentation results. Image artifacts, relative thicknesses of the layers, and similar features across material layers all contribute to the difficulty of identifying the bondline automatically across a large number of specimens. Open-source foundational models provide automatic image segmentation capabilities that can be applied to optical microscopy data sets. In particular, a commercially developed open-source segmentation model was applied to segmenting the layers in bonded structures consisting of Aluminum 7075 adherends. Bondline thickness estimates from full-field optical microscopy were compared against manual point estimates obtained from high-resolution optical microscopy. Finally, random perturbations of the positions of the prompts used to train the model were used to understand the sensitivity of the bondline thickness estimates to the labels.

List of Figures

1 Introduction

An impediment to the adoption of bonded structures for use in aerospace applications is the lack of a reliable nondestructive technique to assess bond strength. Building on the work of [1], a phase-based ultrasonic testing (UT) technique was introduced by [2, 3] to measure interfacial stiffness (viz. chemical bonds per unit area) and evaluated against apparent bond strength measurements taken for specimens comprised of borosilicate glass adherends bonded together using an ultraviolet (UV) cured adhesive. To successfully move toward more complex and aerospace-relevant adherends such as metals or carbon fiber reinforced polymers (CFRPs), a detailed understanding of sources of uncertainty on the phase-based interfacial stiffness model is required since metal or CFRP adherends do not exhibit the same level of uniformity of glass adherends. Bondline thickness, porosity, and acoustic attenuation are all known to impact the predictions of interfacial stiffness using the phase-based UT technique [4], and so methods to automatically assess these bond characteristics are under development. In this paper, image segmentation from full-field optical microscopy (FF-OM) images was used to estimate bondline thickness across the length of six sample specimens comprised of Al 7075 adherends with varying bondline thicknesses ranging from 30 to 260 μm. To validate the analyses, bondline thickness values at discrete locations were obtained manually from high-resolution optical microscopy (HR-OM) that was obtained at 0.53 μm per pixel. A sample specimen is shown in Figure 1.

2 Results and Discussion

For validation purposes, HR-OM estimates of bondline thickness were collected manually at 10 locations across the length of each specimen at approximately 2.5 cm intervals. The locations of the optical microscopy measurements were marked using black ink, which can be seen in the images in Figure 1. The six specimens had nominal bondline thicknesses of approximately 30, 175, and 225 μm, respectively, as indicated in Figure 2.

To compare the analysis of the FF-OM images across the entire lengths of the

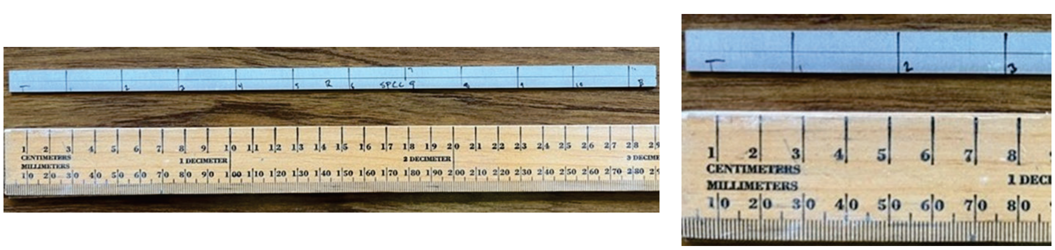

(a) (b)

Figure 1: (a) Full-field image of a bonded specimen approximately 30 cm long and 1 cm wide comprised of Al 7075 adherends with approximate bondline thickness of 225 μm. (b) Detailed image showing locations marked in black at which measurements of bondline thickness were determined using high-resolution optical microscopy.

specimens, composite images were formed from overlapping FF-OM images that were obtained at approximately 7.75 μm per pixel resolution. The pixel size was selected to resolve the bondline and for practical image size constraints. The composite images were created by optimizing cross-correlation [3]. Due to the geometry of the specimens, the resulting composite images of the specimens exhibited extremely high aspect ratio of approximately 40,000 by 850 pixels.

To overcome challenges associated with segmentation of high aspect ratio, each composite image was then split into adjacent square tiles, forming a movie that could be segmented frame-by-frame. The tiling-by-squares approach also brought the shape of the input data closer to the input resolution (1024 by 1024 pixels) employed by the segment anything model 2 (SAM2) [5], which was used for the task of image segmentation. SAM2 has robust capabilities to segment objects in a sequence of images (or frames when referring to video) by tracking the object or feature via the propagation of the initial prompts, which highlight the regions of interest (ROIs). The prompting occurs only in the first image (or frame). The prompt propagation allows the inference process to apply to the rest of the images (or frames). Refinement can be achieved by adding additional prompts to remove areas outside the ROI.

An example composite image cropped to approximately the first 15 cm of an example specimen is displayed in Figure 3(a). Also shown are the first tile (i.e., video frame), positive (green box enclosing the bondline) and negative (red stars) prompts, and the resulting bondline segmentation of a subsequent frame approximately half-way across the length of the specimen (Figures 3(b), 3(c), 3(d), respectively).

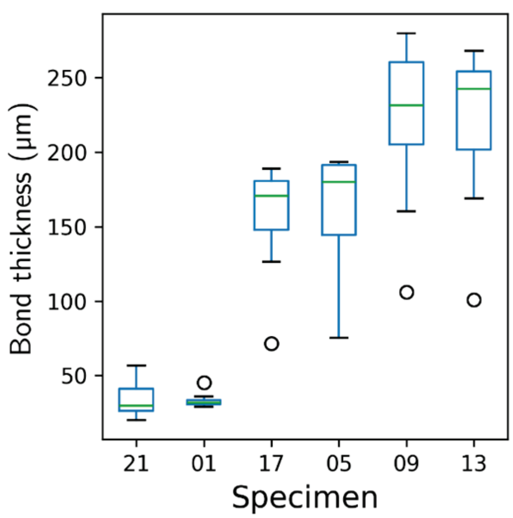

(a)

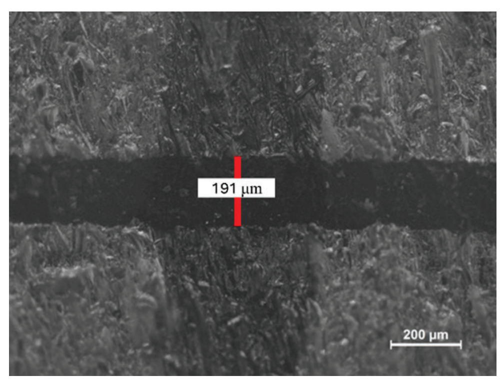

(b)

Figure 2: (a) Distribution of bondline thickness estimates across the lengths of the alloy samples that were obtained from high-resolution optical microscopy. Outliers indicated by open circles. (b) Sample microscopy image with manual bondline thickness measurement.

(a)

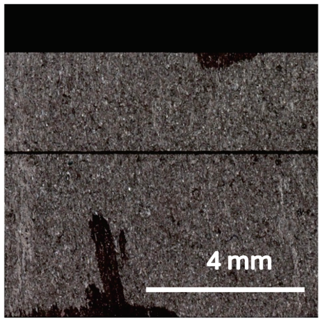

(b)

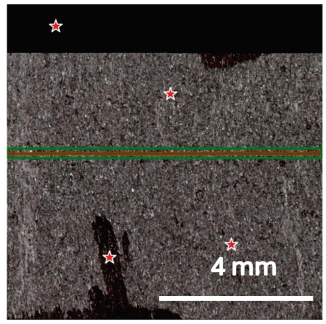

(c)

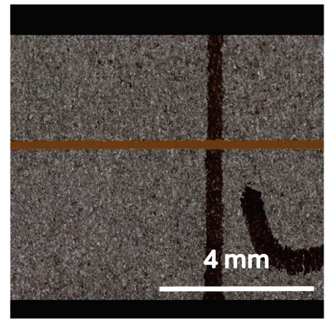

(d)

Figure 3: (a) Composite image formed from overlapping FF-OM images of approximate pixel resolution of 7.75 μm resulting in an FF-OM image of approximately 40,000 by 850 pixels. (b) Tile corresponding to the highlighted blue box in the composite image shown in detail. (c) Positive (green box) and negative (red stars) prompts for the bondline region. (d) Mask of the bondline region obtained from image segmentation of the tile shown with the red box in (a).

To obtain a numerical estimate of bondline thickness, pixels corresponding to the bondline were summed across the vertical direction of the segmented composite image, and a rolling average was computed with a window size of approximately 2 mm in length. A rolling standard deviation in bondline thickness estimates was also computed for each specimen using a 2 mm length rolling window. The results show that most of the manual measurements obtained from HR-OM [Figure 4(a)] lie within one standard deviation of the automated estimate obtained from image segmentation.

Root mean squared error (RMSE) across the entire lengths of the specimens was also estimated by comparing the rolling bondline thickness averages with linear interpolations of the HR-OM values. Based on the RMSE results, the SAM2-predicted bondline thickness estimates agree with the manual HR-OM measurements to within 12 μm, or less than 2 pixel-lengths. In all cases the automated predictions correctly capture the trends in the bondline thickness data.

The final analysis of the method considered the effect of the location of the corner points of the bounding box (or positive prompt) containing the bondline region in the first frame of the movie representation of the bonded specimens. For this, the corner points were randomly perturbed in the vertical direction by a random number of pixels drawn uniformly from 0 to 25 pixels. For each of these 30 trials, the RMSE value across the specimen was computed. The results show the interquartile range for RMSE values vary from approximately 0.4 to 3.5 μm (Figure 5). The variation in errors is greatest for the specimens with smallest nominal bondline thickness values of approximately 30 μm, or 4 pixel-lengths.

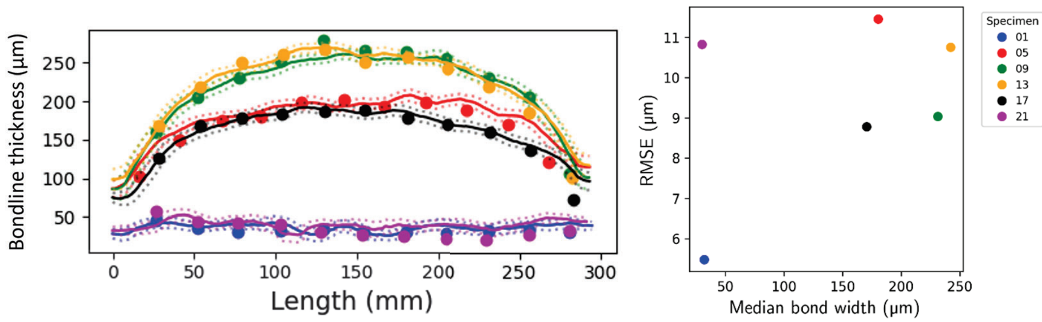

(a) (b)

Figure 4: (a) SAM2 bondline width estimates (solid) for each specimen together with uncertainty bounds (dashed) and manual HR-OM measurements (filled circles). (b) Root mean squared error (RMSE) of automatic estimates across the entire length of each specimen.

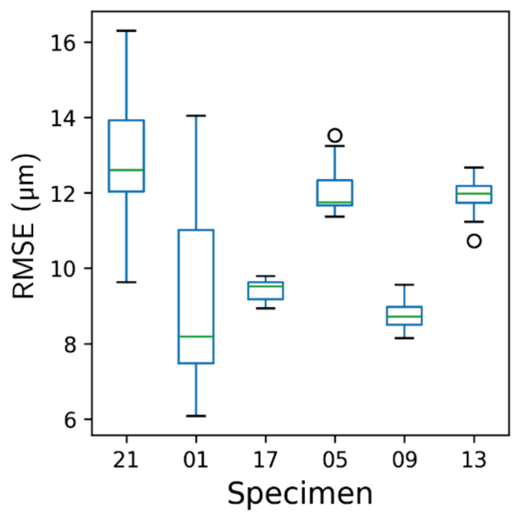

Figure 5: Distributions of root mean squared error (RMSE) values for each alloy sample across 30 random perturbations of the corner points of the bounding box used to label the bondline in the initial frame for bondline image segmentation.

3 Conclusions

Open-source models for image segmentation are a promising tool for characterizing bondline thickness from optical imagery. Treating high aspect ratio images as videos consisting of frames made up of adjacent tiles is a versatile approach to formatting image data to be segmented using segmentation models that propagate prompts across a video or sequence of images since regions of interest need only to be identified in the first image or frame. In this study, the results of the segmentation were shown to be accurate, with a pixel accuracy range from 1.1 to 1.6 pixels, even though the ground truth data obtained from HR-OM were collected at locations that were obscured by a marker. Random perturbations of the prompt containing the bondline showed that the results are not sensitive to this manual step in the analysis relative to the overall level of accuracy obtained with automatic segmentation. Finally, a natural next step is to adapt the method to volumetric X-ray computed tomography measurements with the goal of improving nondestructive methods for assessing the strength of composite bonds.

References

[1] J. Cantrell. "Assessment of adhesive bond strength from ultrasonic tone-bursts". In: *J. Nondestr. Eval.* 37.4 (2018). DOI: `https://doi.org/10.1007/s10921-018-0530-0`.

[2] H. Haldren et al. "A constant-frequency ultrasonic phase method for monitoring imperfect adherent/adhesive interfaces". In: *Ultrasonics* 120 (2022), p. 106641. DOI: `https://doi.org/10.1016/j.ultras.2021.106641`.

[3] S. Preibisch, S. Saalfeld, and P. Tomancak. "Globally optimal stitching of tiled 3D microscopic image acquisitions". In: *Bioinformatics* 25 (2009), pp. 1463–1465. DOI: `https://doi.org/10.1093/bioinformatics/btp184`.

[4] M. Webster, P. Spaeth, and T. Hudson. *Sources of uncertainty in ultrasonic phase-based assessment of interfacial stiffness in adhesive joints*. Presented at the ASNT Research Symposium. Pittsburgh, PA. 2024. URL: `https://ntrs.nasa.gov/api/citations/20240007751/downloads/Webster_Uncertainty%20in%20PBUT_V2.pdf`.

[5] N. Ravi et al. "SAM 2: Segment anything in images and videos". In: *arXiv preprint* (2024). DOI: `https://arxiv.org/abs/2408.00714`.